



Design and manufacturing of high-performance prostheses with additive manufacturing and fiber-reinforced polymers

Daniel-Alexander Türk¹ · Halldór Einarsson¹ · Christophe Lecomte² · Mirko Meboldt¹

Received: 27 September 2017 / Accepted: 18 January 2018 / Published online: 1 February 2018
© German Academic Society for Production Engineering (WGP) 2018

Abstract

This paper presents an approach combining additive manufacturing (AM) with carbon fiber reinforced polymers (CFRP) in an autoclave prepreg process for the development of complex-shaped hybrid AM-CFRP structures with the potential for individualization. The goal of this paper is to investigate the processing route in the context of low volume industrial applications and to assess the mechanical performance of hybrid AM-CFRP structures in ultimate strength and fatigue. The approach was applied to lower-limb prostheses using dissolvable in-autoclave tooling made of ST-130 by fused deposition modeling, two load introduction elements made of titanium by selective laser melting, and pre-impregnated carbon fiber reinforcements. The parts were cured in an autoclave at a pressure of 3 bar and a temperature of 110 °C. The inner toolings were dissolved in a basic solution after curing. The prostheses were subjected to ultimate strength and fatigue tests to assess the mechanical performance of the structures. Results show that the target load of 5474 N was exceeded by 40% and that no fatigue failure occurred for the given loading. Weight savings of 28% compared to a state-of-the-art aluminum reference part were achieved. Results demonstrate that the combination of technologies could be appropriate for high-performance lightweight components with complex geometries.

Keywords Additive manufacturing · Fiber-reinforced polymers · Prosthesis

1 Introduction

Orthoses and prostheses (O&P) are artificial devices that help people with disabilities. Orthoses are externally applied devices that modify the structural characteristics of the neuromuscular skeletal system, whereas prostheses replace missing body parts [1].

There are pre-fabricated and custom-made O&P, with the latter having a better fit to the patient's body and performing better in terms of custom-fit [2].

The development process of custom O&P can broadly be divided into four main steps: geometry capture, device design, device manufacture, fit device to patient. The traditional process for the fabrication of custom O&P uses

manual plaster-molding techniques which are labor-intensive and have long lead times.

Recently, additive manufacturing (AM) has been adopted in the development of custom O&P. AM shows a clear potential in the direct production of individualized products. AM has been used for the production of custom foot orthoses, and studies report on an improved comfort of the insoles and a more evenly distributed pressure over the foot [3, 4]. Costs of solutions using plastic AM are comparable to traditional techniques [5]. Moreover, compared to traditional plaster methods, a digitalized design chain is a faster way to create custom sockets: The geometry of the residual limb is captured using 3D scanning, the data is then converted into surface geometry, the socket is designed using a CAD software and is directly produced with AM [6].

Although AM has made custom prosthetic devices more accessible, polymeric parts made by AM lack durability and strength. In particular, load-bearing devices for active users require high stiffness and strength at low weight. In this context, fiber-reinforced polymers (FRP) are desirable high-performance materials with excellent durability as well as stiffness- and strength-to-weight ratios. The combination

✉ Daniel-Alexander Türk
dtuerk@ethz.ch

¹ Product Development Group Zürich, Department of Mechanical and Process Engineering, ETH Zurich, 8092 Zurich, Switzerland

² Össur Iceland ehf, Grjóthals 5, 110 Reykjavik, Iceland

of AM with FRP offers design opportunities for individualized high-performance lightweight structures. Current applications combining AM and FRP include layup tooling [7–9] and structural lightweight AM elements with added functionalities such as AM honeycombs [10] or load introduction elements [11].

In the context of O&P, Leddy et al. [12] proposed a fabrication method for custom FRP prostheses using AM layup molds in a multi-stage process. A prosthetic finger with integrated functional elements such as pin and flexural joints and urethane grip pads was produced. The shell is made in a wet layup process using carbon fiber that is cured at room temperature. The authors mention the presence of voids in the laminate as a result of the wet layup manufacturing process route which weaken the mechanical performance of the composite part.

To produce high-performance FRP parts, the autoclave prepreg process is a suitable manufacturing technique [13]. In this process, pre-impregnated fiber reinforcements (prepregs) are laid on a tool in the desired fiber orientation. The layup is vacuum-bagged and cured in an autoclave at high pressures and temperatures ranging from 80 °C up to 180 °C [14]. This process allows the manufacture parts with a high fiber volume content and low porosity; however, the elevated curing temperatures and pressures challenge the stability of 3D-printed plastic molds.

In previous work we proposed two approaches for the autoclave processing of hybrid lightweight structures.

In the first approach, a water-soluble sand core made by binder jetting was used in combination with CFRP prepreg to produce a complex hollow lightweight robot structure [15]. In the second approach, a design concept for an aircraft instrument panel consisting of a sandwich structure with multi-functional core elements made by selective laser sintering (SLS), 42 steel inserts made with selective laser melting (SLM), and CFRP prepregs was cured in the autoclave to produce the highly integrated structure [16]. Both studies show weight savings by 54 and 40% compared to reference structures, but mechanical testing did not occur.

To the best of our knowledge, there is no mechanically verified manufacturing route for the autoclave production of hybrid load-bearing parts made of FRP and AM.

In the context of O&P most studies apply AM either on foot or hand orthoses and on lower-limb sockets [17]. Even though the relation between device weight and energy cost of the user is not yet fully understood, most prosthetists agree that lower-limb prosthetics also should be as lightweight as possible to minimize the muscular effort required during locomotion [18]. It is assumed that more energy is required to move a heavier prosthesis during the swing phase. Further consequences of heavy devices are spatial and temporal asymmetries between the prosthetic and the intact limb during gait [19].

In this research, we propose to extend the approach of combining FRP with AM to the development of a mechanically verified, high-performance lower-limb prosthetic knee. The approach uses SLM of titanium powder for the production of load introduction elements (LIE), fused deposition modeling (FDM) of ST-130 for the production of the layup tooling, and SLS of a functional element. The AM components are assembled and over-laminated with carbon-fiber-reinforced polymer prepregs and cured in an autoclave process to form a highly integrated lightweight part. Ultimate static and cyclic strength tests were conducted to assess the mechanical performance of the novel lower-limb prosthesis.

This study should provide comprehensive knowledge in the design and manufacturing of high-performance parts made of FRP and AM.

2 Background information

2.1 Selective laser melting (SLM)

Selective laser melting (SLM) is a powder-bed fusion process where a laser beam selectively melts the metallic powder material. The powder particles in the scanned area are consolidated resulting in a nearly fully dense layer of the part being built. The powder bed is lowered by thickness of a layer and a coater applies another layer of powder material to the bed. The process is repeated until the final physical part is produced [20]. Residual stresses may cause part distortions, crack formation, or reduce the fatigue performance of the part [21]. To counter these challenges, support structures are required and heat treatment or hot iso-static pressure may be applied to relieve any residual stresses. Novel scanning strategies, numerical models of the thermo-mechanical material behavior during the process and design strategies may be applied to reduce residual stresses [22–25].

2.2 Selective laser sintering (SLS)

Selective laser sintering (SLS) is a powder-bed process where a laser selectively melts thermoplastic powder material in the scanned area [26]. Common materials used in SLS are polyamide 11, polyamide 12, or compounds of PA12 [27]. In contrast to SLM, the melting of PA12 does not require such high energy density inputs. The surround powder acts a support during the building procedure, and therefore SLS offers the possibility to produce complex geometries without any explicit supports [28].

2.3 Fused deposition modeling (FDM)

In fused deposition modeling (FDM), a filament is fed through a heating element and extruded through a nozzle

onto the building platform [29]. Acrylonitrile butadiene styrene (ABS), polylactide (PLA) and polycarbonate (PC) are common materials for FDM; however, today a new class of materials including particle [30, 31], short [32], or continuous fiber reinforcements [33] are being developed. FDM requires support structures for overhangs which are mechanically removed or chemically dissolved after manufacture. Material properties are anisotropic as a result of process factors including directional deposition of the filament, air gap, bead width, model build temperature and raster orientation [34].

3 Materials and methods

3.1 Reference part: Mauch knee

The Mauch knee depicted in Fig. 1 (left) is a passive knee that uses a hydraulic cylinder to provide support during the stance and returns to an extended position during the swing phase. The Mauch knee weighs 1.14 kg, while the load-bearing frame weighs 338 g. The knee is rated for active users weighing up to 136 kg. It is produced in low to mid volumes [35].

The aluminum frame is a machined part (in black), that is covered with non-loadbearing plastic elements (in white). A movable part is mounted on top of the knee to provide an attachment point to the socket. At the bottom, a metallic stud is mounted providing a connection to the pylon. The Mauch knee is a complex load-bearing part with integrated attachment points, which makes it very suitable from a technical perspective for a redesign with AM and FRP.

3.2 Load cases

The structure is subjected to static and cyclic loading to verify its durability. The ultimate strength of the frame is assessed in accordance with the standard ISO 10328:2006 [36]. The standard defines two static loading conditions that are heel strike and forefoot loading. In this study, the forefoot loading induced higher stresses in the structure, which is why it was considered to be the critical load case. In this load case an eccentric static load of $F_T = 5474$ N is introduced into the test set-up, corresponding to an additional safety factor of 36% to the test force, which is an internal safety factor defined by Össur Iceland ehf. The geometrical configuration in accordance with the standard is shown in Fig. 1, right. The load is introduced into the structure using two levers (top view) which allow for the specific arrangement according to the parameters of the load case.

A cyclic test was conducted in accordance with ISO 10328:2006. With a test frequency of 6 Hz a load between 50 and 1614 N is applied on the structure for a minimum of $n = 3 \times 10^6$ cycles. Then, a final static proof force of 2780 N is applied to verify the residual strength of the structure.

3.3 Design concept

The design concept combines the strengths of both the AM and the prepreg layup technologies. FRP are materials with outstanding stiffness- and strength-to-weight ratios if the fibers are oriented in the direction of the load. However, the manufacturing of FRP parts requires tooling. Traditional toolmaking is costly and characterized by long lead times. AM, on the other hand, allows the direct production of complex-shaped tooling from digital data. For FRP

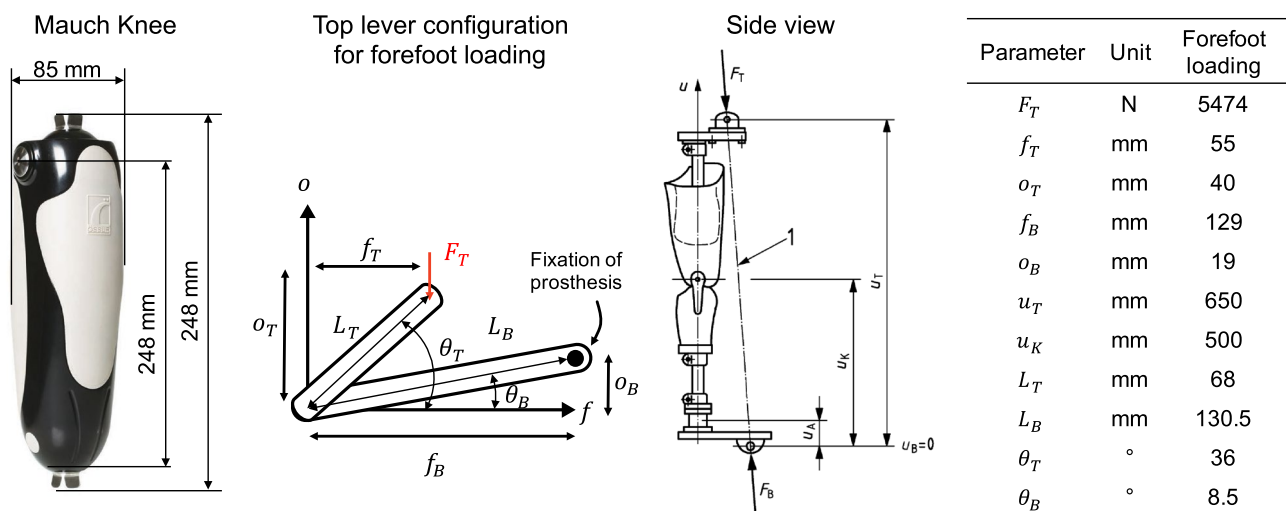


Fig. 1 Mauch knee [35] (left) and forefoot loading parameters according to ISO 10328 [36] (right)

laminates, the integration of additional functionalities is possible with embedded functional layers. Typical functions include damping, toughness, electrical and/or thermal conductivity, sensing, actuation [37] but also lightning strike [38] and icing protections [39]. However, the integration of three-dimensional design features with a defined geometry is more difficult, such as it is the case for load introduction, positioning and fixation elements. Here, the geometric freedom provided by AM is advantageous as complex functional and load-bearing elements can be designed into one single part. A division of tasks follows: FRP are used in areas that require high strength and stiffness at low weight, e.g. load-bearing shells, while AM is used in areas where high geometrical complexities with additional functionalities are necessary.

The design concept of the lower-limb prosthesis depicted in Fig. 2 includes two load introduction elements (LIE), a functional element, and a soluble tooling made by AM, and a thin shell made by CFRP.

The two LIE (grey) connect the knee to the upper socket and the lower pylon. They host bearing seats with tight tolerances, a stopper, and a stud. Therefore, they are made by metal SLM. The load is introduced into the bearing seats and transferred into the CFRP laminate via the bonding surfaces. A film adhesive with a defined thickness is used to provide sufficient shear strength to transfer the load into the CFRP shell. The middle section (yellow) consists of a light and stiff CFRP prepreg shell. To manufacture such a curved structure, a soluble inner core is made by FDM. The inner core (red) features form fits for the assembly of the load introduction elements and a pocket for the insertion of a functional mock-up element (green). The functional mock-up element contains design features such as snap-fit joints for the fixation of housing elements or electronics which may be connected to the structure after curing. In study the co-curing to the CFRP shell and functionality of the snap-fits is tested. It may be produced with FDM or SLS, depending on the specific functional requirements and the curing cycle. Two silicone molds are used to compact the CFRP laminate during curing and to minimize wrinkles.

3.4 Detailed design

Figure 3 shows the detail design of the upper and the lower LIE made by SLM. The section views show the as-built versions with temporary machining and processing aids depicted in purple. Supports structures connect the load transfer surfaces and therefore reduce the warping of the sides. Furthermore, they reduce vibrations of otherwise free edges during machining. To counter process-induced inaccuracies, a material offset is used at the location of the bearing seats. To reduce the amount of support material, tear-drop shapes are used for the vibration support and the

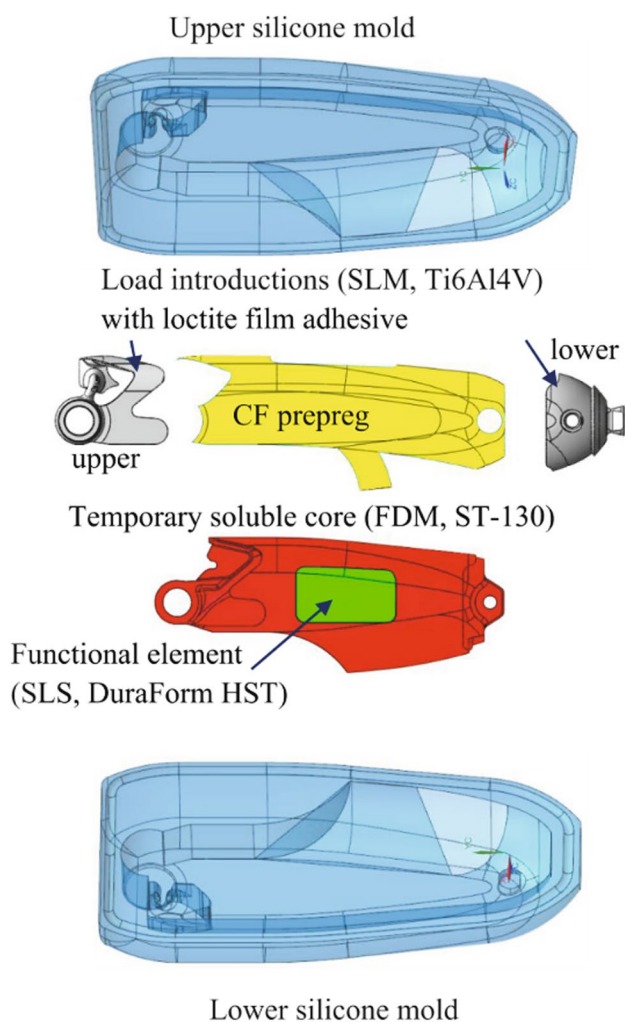


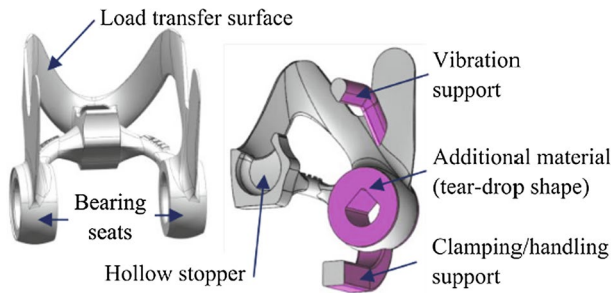
Fig. 2 Design concept for the lower-limb prosthesis

bearing seats. The additional material is then removed by machining. To save weight, hollow sections are included in the stopper of the upper part and in the stud of the lower part. An elliptical channel with two three millimeter powder extraction holes revolves around the stud. Load transferring surfaces are designed in such way to maximize the bonding surface to the CFRP material resulting in a 0.8 mm thin surface which is reinforced with an integrated stiffener.

The inner core (Fig. 4) is made by FDM. It features contact surfaces with an offset of 0.2 mm for the pre-assembly of the LIE and hosts the functional element that is plugged into the core using integrated snap-fit joints.

The CFRP layup consists of a symmetric base layup including prepreg fabrics and unidirectional plies. A total number of 14 plies is used, resulting in a thickness of 2.26 mm. The sides are reinforced with 18 plies, resulting in a thickness of 2.82 mm.

(a) Upper load introduction element



(b) Lower load introduction element

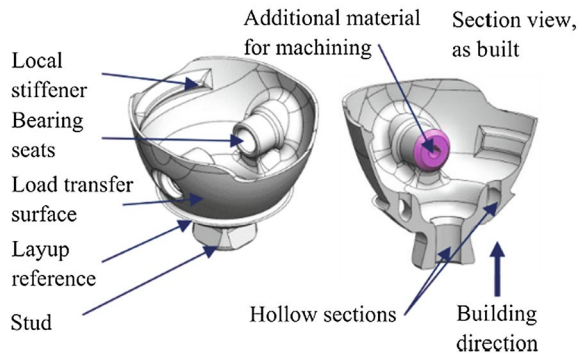


Fig. 3 Detail design of the upper (a) and lower (b) load introduction elements as-built and machined

3.5 Materials properties

Ti6Al4V by Concept Laser was used for the LIE made by SLM due to its excellent strength-to-weight ratio of around 260 kNm/kg [40]. Static material properties were taken from the data sheet. The inner core is made of ST-130, a soluble plastic for FDM processes, currently in development by Stratasys Ltd [41]. The material is developed for

in-autoclave tooling applications and is claimed to be stable up to 121 °C at a pressure of 3 bar and up to 98 °C at 6 bar. For the functional element, DuraForm HST Composite by 3D Systems was used due to its acceptable mechanical performance at elevated temperatures [42]. For the composite layup the uni-directional SIGRAPREG C U150-0/NF-E340/38% [43] and the fabric SIGRAPREG C W200-TW2/2-E323/45% [44] provided by SGL Group were used. A Loctite EA 9686 AERO [45] epoxy film adhesive was used to bond the SLM parts to the composite. Table 1 shows the material properties.

3.6 Manufacturing

The manufacturing route consists of a sequential combination of selected AM techniques with the autoclave prepreg process. It is illustrated in Fig. 5.

Two LIE were manufactured by SLM in a Concept Laser-Cusing machine by 3D Precision SA, Switzerland. The parts were removed from the building platform. The bonding surfaces were covered during the sand-blasting operation to retain the as-built surface roughness of the SLM. The as-built surface roughness was measured on a SURFCOM FLEX 50A machine by Zeiss and the arithmetic average R_a amounted to 10.5 μm . To relieve residual stresses, the parts were heat-treated in a chamber filled with argon gas. The parts were heated at a rate of 5°C/min, held for 2 h at 840 °C, and cooled down at a rate of 1°C/min to 500 °C, resulting in a total cycle time of 12 h. The SLM parts were then clamped and machined to remove the temporary support structures.

The inner core was manufactured on a Fortus 900mc by Stratasys using an extrusion nozzle with a resolution of 0.330 mm. The inner core was hand-sanded using 120 and 300 grit sand paper to smoothen the surfaces. It was sealed with Super Seal from Smooth-On [46] to prevent the resin inflow into the FDM part during curing.

Fig. 4 Inner core by FDM with contact surfaces for the preassembly of the load introduction elements (left) and CFRP layup (right)

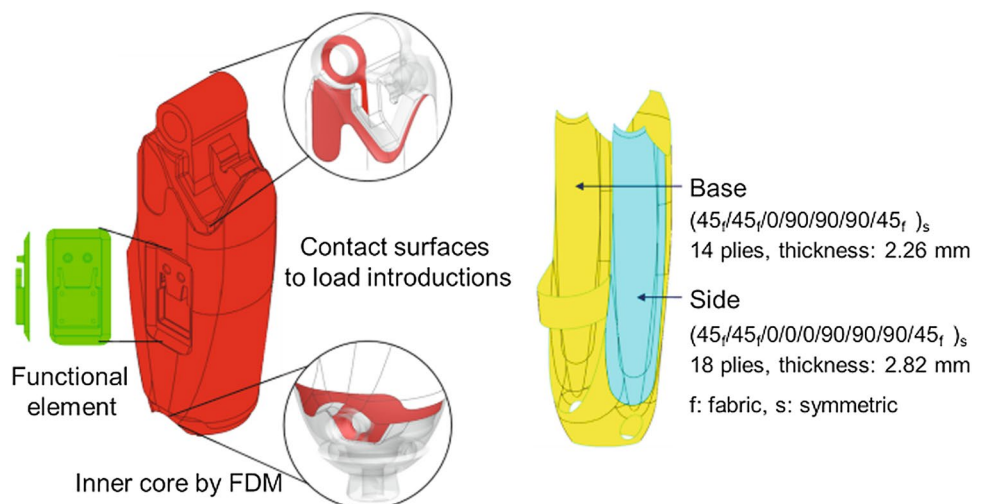
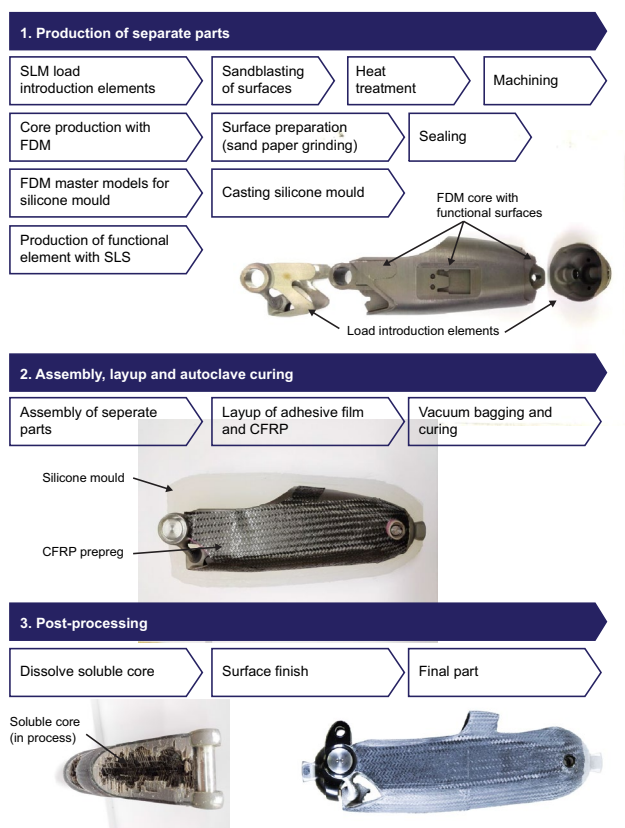


Table 1 Material properties from spec sheets

Material	Parameter	Value	Unit
Ti6Al4V	Young's modulus	~ 110	GPa
	Yield strength (upright)	989	MPa
	Tensile strength (upright)	1071	MPa
UD	Young's modulus 0°	140	GPa
	Young modulus 90°	8.4	GPa
	Shear modulus	5200	GPa
	Poisson ratio	0.318	
	Tensile strength 0°	2400	MPa
	Inter-laminar shear strength	90	MPa
	Fabric	Young's modulus 0°	62
	Young's modulus 90°	60	GPa
	Shear modulus	4670	GPa
	Poisson ratio	0.03	
	Tensile strength 0°	950	MPa
	Tensile strength 90°	900	MPa
	Inter-laminar shear strength	68	MPa
Loctite	Shear strength	40.7	MPa

**Fig. 5** Manufacturing route

A two-piece outer mold was cast using ProtoSil RTV 245 silicone from Altropol [47]. The silicone was cast into a master mold made by FDM. The functional element was produced by SLS.

The single elements were then pre-assembled using the complex form fits designed into the FDM tool. The CFRP prepregs were laminated onto the assembly. A film adhesive was placed between the SLM elements and the prepreg. The assembly and the layup were covered with the silicone mold. The mold was wrapped in breather material and vacuum bagging was applied. The part was then cured in an autoclave: It was heated at a rate of 1°C/min up to 110 °C, held for 200 min and cooled down at a rate of 1°C/min. Vacuum and 3 bar autoclave pressure were applied during the process. After curing, the part was demolded and the inner core was dissolved for 15 h in a circulation tank containing a heated alkaline solution.

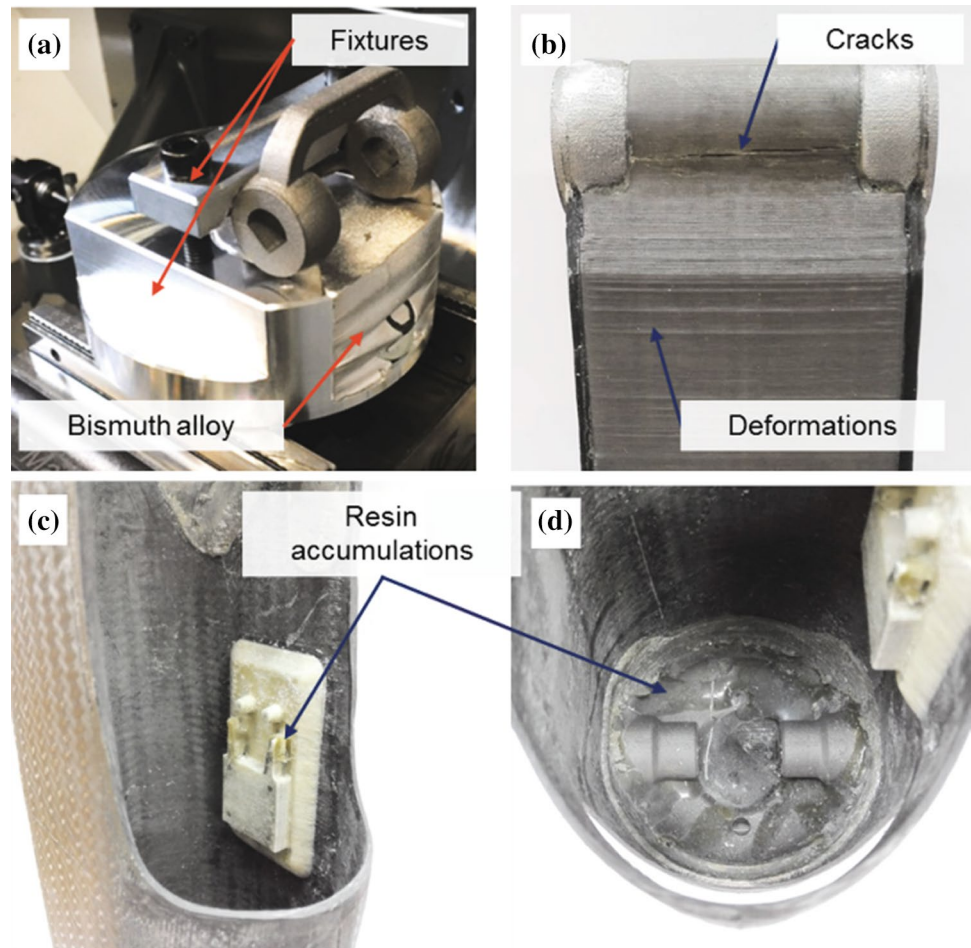
4 Results

4.1 Manufacturing results

The clamping and machining of AM parts require particular attention if the geometry is complex, contains thin walled structures, and if the material is rigid. These conditions were taken into account during the design phase by including vibration supports. However, the upper SLM part could not be clamped in a satisfactory way, as necessary clamping forces could not be applied without facing the risk of distorting the part. To increase the clamping stability, a bismuth alloy [48] with a low melting point of 70 °C was melted over hot water and poured into the fixture containing the titanium part. The bismuth alloy solidified in the fixture and provided a continuous load transfer of the machining forces throughout the whole structure into the vice (Fig. 6a). After the machining, the titanium part and the fixture were placed in a 90 °C hot water bath for 15 min to melt away the bismuth alloy leaving no residual bismuth on the titanium or on the fixture.

Cracks between delaminated printing layers were observed after curing in the FDM core (Fig. 6b). Moreover, deformations of the core structure were observable; however, they were considered to be of minor relevance to the functionality of the part. These effects may have been caused by thermal residual stresses which may be a result of the coefficient of thermal expansion of the thermoplastic material ranging between 76 and 177 $\mu\text{m}/(\text{m } ^\circ\text{C})$ depending on the orientation of the filaments. Moreover, the CTE of the thermoplastic material is significantly higher than the CTE of CFRP. Also, the combination of thermal and pressure loading might have caused the cracks and deformations. Resin accumulations were found in gaps and cavities, e.g. in

Fig. 6 Clamping of the upper load introduction element (a) using aluminum fixtures and a bismuth alloy, cracks in the FDM core after autoclave processing (b), resin accumulations at the snap-fit (c) and in the lower load introduction element (d) after core washout



the snap-fit element (Fig. 6c) and in the lower load introduction cavity (Fig. 6d). They require manual removal during post-processing. Particular attention is therefore recommended to seal gaps and close cavities. The FDM mold was washed out completely, which indicated that the resin did not flow into the core. The co-curing of the functional element was successful, and the resin formed a load-bearing bonding between the CFRP and the functional element. The part did not show any wrinkles or dry spots in the reinforcement layers, indicating that using a silicone mold is a suitable technique for distributing the pressure on complex geometries during the curing stage.

4.2 Ultimate strength test result

The ultimate strength test set-up is shown in Fig. 7. The structure failed at the interface of the lower LIE to the CFRP reinforcement at a load of 7685 N, which corresponds to approximately 140% of the targeted load. A mixed failure mode including adhesive, cohesive and laminate failure is observed. Adhesive failure areas are

small and found to be close to the edge of the SLM part. A larger area shows cohesive failure which is recognizable by adhesive residues. The mechanical loading condition consists of a combination of bending and compression. It is assumed that the compression loading induced shear stresses at the interface of the CFRP to the lower metal part. The shear stresses should ideally be distributed across the entire surface area of the adhesive film [49]. However, in combination with the bending loading, a peel-effect may have occurred. In such effect, the peel stresses are concentrated at the edge of the metal-CFRP interface, limiting the total interface strength to a very small zone of the adhesive. This effect could have led to adhesive failure near the edge of the SLM part. The failure types observed in the laminate are delamination and fiber fracture. Delamination may have occurred as a result of the peel-effect which probably induced high transverse shear stresses. In order to predict the failure mode in detail, a simulation model including the adhesive layer and failure mechanics for the CFRP and the adhesive layer is necessary. No damage was observed at the SLM part.

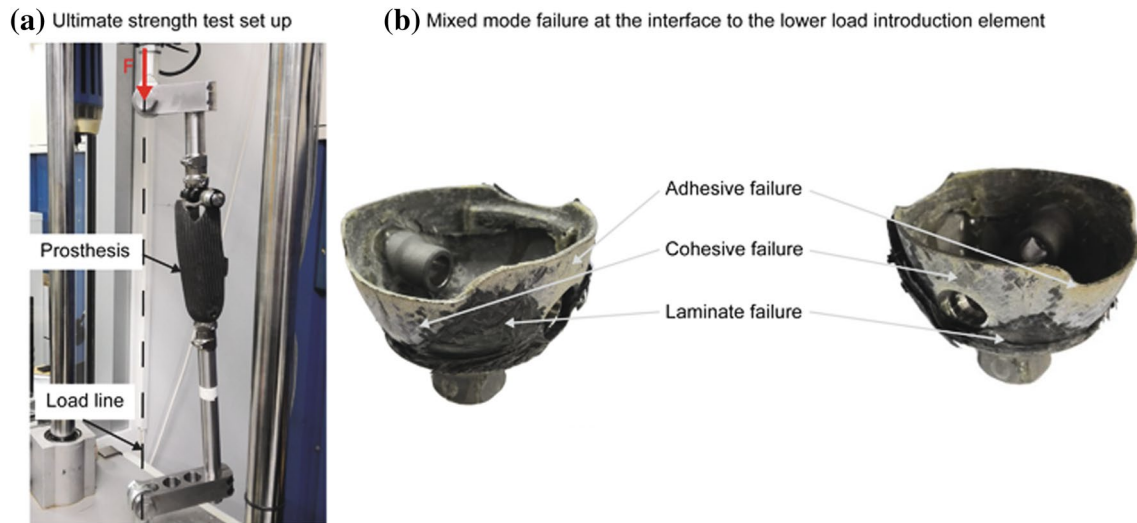


Fig. 7 Ultimate strength test set-up (left) and mixed failure at the interface of the lower load introduction element and the CFRP

Table 2 Test log of the cyclic test of the hybrid structure

Stress cycles n	u ($F_{\min} = 50$) (mm)	u ($F_{\max} = 1614$) (mm)
2500	0.00	2.30
389,000	0.00	2.30
905,500	0.00	2.30
1,430,500	0.09	2.21
1,579,500	0.09	2.21
3,022,000	0.01	2.29

4.3 Fatigue test result

The second prototype passed the fatigue test, which was aborted after reaching more 3×10^6 cycles without any significant change in the displacement or any observable failure of the structure. Table 2 shows the number of cycles as well as the deformation at a minimum load of 50 N which represents the calibration load, and at a maximum load of 1614 N.

4.4 Weight

The final prototype weighs 262 g, consisting of 80 g for the upper and 72 g for the lower titanium LIE, and 110 g for the CFRP. The weight of the mock-up element is excluded in this calculation. This corresponds to a weight reduction by 28% from the reference weight of 338 g. With optimizations, we expect to save a further 20% resulting in a total weight of approximately 210 g, which would correspond to total weight savings of around 38%.

5 Discussion

The thermoplastic material ST-130 was used for the production of the soluble tooling. At the time of this research, the material was still under development such that, even though the material was successfully employed, some limitations became evident: The exposure of the material to elevated temperatures and pressures over a cycle time of several hours can lead to creeping and residual stresses. The thermo-mechanical stability of the polymeric material is a critical factor in the design and processing of hybrid parts made by AM and FRP. Lowering the curing conditions may be an option to minimize deformations. However, lower curing temperatures increase cure cycle times and low pressures may lead to an increase in voids, thus affecting the mechanical performance. Binder jetting of water-soluble silica sand could be an alternative and more cost-efficient technique for the production of inner tooling. Silica sand, for example, is a material that shows low thermal expansion and a high melting temperature [50, 51]. The main advantage of the FDM core is the possibility to integrate defined design features (e.g. positioning and fixation features) which allow to position additional functional elements to the CFRP prior to curing. The selection of 3D printing technology and materials therefore is a compromise between design freedom, mechanical performance, processing suitability, and costs.

The study has shown that in hybrid structures the interface between the CFRP and the titanium parts is of particular importance in the load transfer. The current bonding design exhibits a stiffness discontinuity at the transition of the CFRP to the titanium parts. A ductile film adhesive with constant thickness was used to reduce the stress peaks. However, AM and the prepreg layup technology offer the potentials to design

a bonding area with quasi-equal stiffness. Various design parameters are available to tune the stiffness such as materials selection, layup design, ply thickness, and orientation. The roughness of AM printed surfaces could also affect the bonding strength. For SLM, the parameters influencing the surface roughness are the building orientation and the post-processing methods such as sand-blasting or roto-finishing. The process-inherent roughness could be beneficial to the bonding strength. Future adhesive joining concepts propose 3D-printed pin reinforcements that mechanically interlock with the fibers to increase the ultimate breaking load.

The proposed manufacturing route involves a high number of steps. The production of the titanium parts requires sand blasting, heat treatment, and CNC machining to provide the part with the desired functionality. Manual work is necessary in the post-processing of the SLM parts (support removal, clamping), and in the FRP layup process. However, the use of AM tooling with added functionalities (e.g. pockets, mounting surfaces) and the integration of AM elements in the course of the layup process results in the manufacturing of a highly integrated structure. After curing, the AM-CFRP structure does not require any additional assembly operations as it is the case for many machined parts made according to the differential design approach. In this study, the stud was integrated in the lower load introduction element, and the whole knee is made of one single part. The reduction of the number of parts through an integral design approach is the lever to reducing weight. The combination of AM with layup of CFRP allows the production of integrated structures with complex geometries and added functionalities.

In the context of O&P, weight plays a significant role in the prosthetic gait. Studies report that people with transtibial amputations require 20–25% more energy during gait, walk slower and take smaller steps compared to able-bodied subjects [52]. The gait adaption is a result of the asymmetry in the inertia mass of the lower limbs. Studies found that matching the mass and the moment of inertia of the prosthetic limb to the intact side by adding weights between 0.85 and 2.6 kg lead to increased energy cost [53, 54]. Weight therefore seems to be one important characteristic among many added functionalities such as powered ankles, vacuum-assisted sockets or hydraulic suspension systems. The possibility to integrate additional functionalities such as sensors, cable ducts, and graded stiffness in combination with lightweight structures, makes the presented approach promising for future applications in the field of individualized O&P.

6 Conclusions

A manufacturing approach combining AM with FRP in an autoclave layup process was presented and applied to lower-limb prostheses. The mechanical performance of the

prostheses were successfully verified in ultimate strength and fatigue tests. The prostheses exhibit weight savings of 28%, with further weight reduction potentials.

Limits of the manufacturing approach are the thermo-mechanical stability of polymeric AM components subjected to autoclave prepreg curing conditions. Load-transferring interfaces between AM components and the CFRP are of particular interest, and an experimental characterization is recommended. Finally, the design engineer should consider the service operation of the part and its manufacturing process during the design phase to fully leverage the advantages AM has to offer. In the near future, the approach could be cost-competitive for individualized, low-volume applications.

Acknowledgements This research was supported by Össur Iceland ehf and the Product Development Group Zurich, ETH Zurich.

References

1. Shurr DG, Michael JW (2001) *Prosthetics and Orthotics*, 2nd edn. Prentice Hall, Upper Saddle River
2. Gailey R, Allen K, Castles J, Kucharik J, Roeder M (2008) Review of secondary physical conditions associated with lower-limb amputation and long-term prosthesis use. *J Rehabil Res Dev*. 45(1):15–30 (<http://www.rehab.research.va.gov/jour/08/45/1/pdf/gailey.pdf>)
3. Salles AS, Gyi DE (2013) Delivering personalised insoles to the high street using additive manufacturing. *Int J Comput Integr Manuf* 26(1):386–400. <https://doi.org/10.1080/0951192X.2012.717721>
4. Salles AS, Gyi DE (2013) An evaluation of personalised insoles developed using additive manufacturing. *J Sports Sci* 31(4):442–450. <https://doi.org/10.1080/02640414.2012.736629>
5. Saleh J, Dalgarno K (2009) Cost and benefit analysis of fused deposition modelling (FDM) technique and selective laser sintering (SLS) for fabrication of customised foot orthoses. In: *Proceedings of 4th international conference advanced research virtual rapid manufacturing, innovative developments in design manufacturing*
6. Jin Y, Plott J, Chen R, Wensmann J, Shih A (2015) Additive manufacturing of custom orthoses and prostheses—a review. *Proc CIRP* 36:199–204. <https://doi.org/10.1016/j.procir.2015.02.125>
7. Li H, Taylor G, Bheemreddy V, Iyibilgin O, Leu M, Chandrashekhara K (2015) Modeling and characterization of fused deposition modeling tooling for vacuum assisted resin transfer molding process. *Addit Manuf* 7:64–72. <https://doi.org/10.1016/j.addma.2015.02.003>
8. Schniepp T (2016) Design guide development for additive manufacturing (FDM) of composite tooling. In: *SAMPE conference proceedings*, Long Beach, CA, pp 2259–2269
9. Love L, Kunc V, Rios O, Duty CE, Elliot AM, Post BK, Smith RJ, Blue CA (2014) The importance of carbon fiber to polymer additive manufacturing. *J Mater Res* 20:1893–1898. <https://doi.org/10.1557/jmr.2014.212>
10. Riss F, Schilp J, Reinhart G (2014) Load-dependent optimization of honeycombs for sandwich components—new possibilities by using additive layer manufacturing. *Phys Proc* 56:327–335. <https://doi.org/10.1016/j.phpro.2014.08.178>
11. Türk DA, Züger A, Klahn C, Meboldt M (2015) Combining additive manufacturing with CFRP composites: design potentials. In:

- Proceedings of the 20th international conference on engineering design (ICED15), vol 8, ISBN: 978-1-904670-71-1
12. Leddy MT, Belter JT, Gemmel KD, Dollar AM (2015) Light-weight custom composite prosthetic components using an additive manufacturing-based molding technique. In: 2015 37th annual international conference of the IEEE Engineering in Medicine and Biology Society (EMBC), Milan, pp 4797–4802. <https://doi.org/10.1109/EMBC.2015.7319467>
 13. Mazumdar SK (2002) Composites manufacturing—materials, product, and process engineering. CRC Press, Boca Raton. (ISBN 0-8493-0585-3)
 14. Gutowski TG (1997) Advanced composites manufacturing. Wiley, Cambridge. (ISBN: 978-0-471-15301-6)
 15. Türk DA, Triebe L, Meboldt M (2016) Combining additive manufacturing with advanced composites for highly integrated robotic structures. In: 26th CIRP design conference vol 50, pp 402–407. <https://doi.org/10.1016/j.procir.2016.04.202>
 16. Türk DA, Kussmaul R, Zogg M, Klahn C, Spierings AB, Ermanni P, Meboldt M (2016) Additive manufacturing with composites for integrated aircraft structures. *J Adv Mater* 3:55–69. (ISSN 1070-9789)
 17. Chen RK, Jin Y, Wensman J, Shih A (2016) Additive manufacturing of custom orthoses and prostheses—a review. *Addit Manuf* 12:77–89. <https://doi.org/10.1016/j.addma.2016.04.002>
 18. Mattes S (2014) Is lighter better? Thoughts on the relationship between device weight and function. *The O&P Edge*. http://opedg.com/Articles/ViewArticle/2014-05_07. Accessed 20 Dec 2016
 19. Lewallen R, Dyck G, Quanbury A, Ross K, Letts M (1986) Gait kinematics in below-knee child amputees: a force plate analysis. *J Pediatr Orthop* 6(3):291–298
 20. Gibson I, Rosen DW, Stucker B (2010) Additive manufacturing technologies. Springer, New York. (ISBN: 978-1-4419-1119-3)
 21. Parry L, Ashcroft IA, Wildman RD (2016) Understanding the effect of laser scan strategy on residual stress in selective laser melting through thermo-mechanical simulation. *Addit Manuf* 12:1–15. <https://doi.org/10.1016/j.addma.2016.05.014>
 22. Zaeh MF, Branner G (2010) Investigations on residual stresses and deformations in selective laser melting. *Prod Eng Res Dev* 4(1):35–45. <https://doi.org/10.1007/s11740-009-0192-y>
 23. Zhao X, Iyer A, Promopattam P, Yao S-C (2017) Numerical modeling of the thermal behavior and residual stress in the direct metal laser sintering process of titanium alloy products. *Addit Manuf* 14:126–136. <https://doi.org/10.1016/j.addma.2016.10.005>
 24. Vastola G, Zhang G, Pei QX, Zhang Y-W (2016) Controlling of residual stress in additive manufacturing of Ti6Al4V by finite element modeling. *Addit Manuf* 12:231–239. <https://doi.org/10.1016/j.addma.2016.05.010>
 25. Leuteneker-Twelsiek B, Klahn C, Meboldt M (2016) Considering part orientation in design for additive manufacturing. *Proc CIRP* 50:408–413. <https://doi.org/10.1016/j.procir.2016.05.016>
 26. Schmid M, Amado A, Wegener K (2014) Materials perspective of polymers for additive manufacturing with selective laser sintering. *J Mater Res* 29(17):1824–1832. <https://doi.org/10.1557/jmr.2014.138>
 27. Schmid M, Amado A, Wegener K (2016) Polymer powders for selective laser sintering (SLS). In: AIP Conference proceedings 1664, 160009. <https://doi.org/10.1063/1.4918516>
 28. Breuninger J, Becker R, Wolf A, Rommel S, Verl A (2013) Generative Fertigung mit Kunststoffen. Konzeption und Konstruktion für Selektives Lasersintern. Springer, New York. https://doi.org/10.1007/978-3-642-24325-7_54
 29. Bellini A, Güçeri S (2003) Mechanical characterization of parts fabricated using fused deposition modeling. *Rapid Prototyp J* 9(4):252–264. <https://doi.org/10.1108/13552540310489631>
 30. Masood SH, Song WQ (2004) Development of new metal/polymer materials for rapid tooling using fused deposition modelling. *Mater Des* 25:587–594. <https://doi.org/10.1016/j.matdes.2004.02.009>
 31. Nikzad M, Masood SH, Sbarski I (2011) Thermo-mechanical properties of a highly filled polymeric composites for fused deposition modeling. *Mater Des* 32:3448–3456. <https://doi.org/10.1016/j.matdes.2011.01.056>
 32. Tekinalp HL, Kunc V, Velez-Garcia GM, Duty CE, Love LJ, Naskar AK, Blue CA, Ozcan S (2014) Highly oriented carbon fiber-polymer composites via additive manufacturing. *Compos Sci Technol* 105:144–150. <https://doi.org/10.1016/j.compscitech.2014.10.009>
 33. Matsuzaki R, Ueda M, Namiki M, Jeong T-K, Asahara H, Horiguchi K, Nakamura T, Todoroki A, Hirano Y (2015) Three-dimensional printing of continuous-fiber composites by in-nozzle impregnation. *Nat Sci Rep*. <https://doi.org/10.1038/srep23058>
 34. Ahn S-H, Montero M, Odell D, Roundy S, Wright PK (2002) Anisotropic material properties of fused deposition modeling ABS. *Rapid Prototyp J* 8:248–257. <https://doi.org/10.1108/13552540210441166>
 35. Össur Iceland ehf (2017) Mauch® Knee specifications. <https://www.ossur.com/prosthetic-solutions/products/all-products/knees-and-legs/mauch-knee>. Accessed 14 Jan 2017
 36. EN ISO 10328 standard, Prosthetics. (2006) Structural testing of lower-limb prostheses. Requirements and test methods
 37. Gibson RF (2010) A review of recent research on mechanics of multifunctional composite materials and structures. *J Compos Struct* 92:2793–2810. <https://doi.org/10.1016/j.compstruct.2010.05.003>
 38. Gagné M, Therriault D (2014) Lightning-strike protection of composites. *Prog Aerosp Sci* 64:1–16. <https://doi.org/10.1016/j.paerosci.2013.07.002>
 39. Mohseni M, Amirfazli A (2013) A novel electro-thermal anti-icing system for fiber-reinforced polymer composite airfoils. *Cold Reg Sci Technol* 87:47–58. <https://doi.org/10.1016/j.coldregions.2012.12.003>
 40. Concept, Laser (2017) CL 41TI ELI Titanium alloy data sheet. https://www.concept-laser.de/fileadmin/user_upload/Datasheet_CL_41TI_ELI.pdf. Accessed 20 Dec 2016
 41. Stratasys, Ltd. (2017) ST-130 datasheet. <http://www.stratasys.com/materials/fdm/st-130>. Accessed 20 Dec 2016
 42. Türk DA, Brenni F, Zogg M, Meboldt M (2017) Mechanical characterization of 3D printed polymers for fiber-reinforced polymers processing. *Mater Des* 118:256–265. <https://doi.org/10.1016/j.matdes.2017.01.050>
 43. SGL Group (2017) Sigratex prepreg CE 1007-15-38 datasheet. <http://www.carbon-vertrieb.com/shop/media/products/0447494001371540646.pdf>. Accessed 10 Dec 2016
 44. SGL Group (2017) Sigratex prepreg C W200-TW/2-E323/45%/3K datasheet. <http://www.carbon-vertrieb.com/shop/media/products/0264600001371540621.pdf>. Accessed 20 Feb 2017
 45. Loctite EA 9686 (2017) AERO, data sheet. http://www.aero-consultants.ch/view/data/3285/Aero%20Consultings/PDF/LOCTITE_EA_9686_AERO.PDF. Accessed 20 Jan 2017
 46. Smooth-On (2017) SuperSeal data sheet. <https://www.smooth-on.com/products/superseal/>. Accessed 21 Jan 2017
 47. Altrapol (2017) ProtoSil RTV 245 silicone data sheet. http://www.altrapol.de/wp-content/uploads/2016/11/E_RTV_245.pdf. Accessed 21 Jan 2017
 48. Witte Weiguss mould clamping technology, bismuth alloy (2017) <https://www.witteamerica.com/products/vacuum/mould-clamping-technology.php>. Accessed 01 June 2017
 49. Davis MJ, Bond DA (1999) The importance of failure mode identification in adhesive bonded aircraft structures and repairs. In: International conference on composite materials ICCM-12, Paris, July 5–9

50. ExOne (2017) Casting media alternatives. <http://www.exone.com/Portals/0/ResourceCenter/Materials/ExOne-Casting-Media-Alternatives.pdf>. Accessed 16 Feb 2017
51. Hackney PM, Woolridge R (2017) Characterisation of direct 3D sand printing process for the production of sand cast mould tools. *Rapid Prototyp J* 23(1):7–15. <https://doi.org/10.1108/RPJ-08-2014-0101>
52. Gailey RS, Wenger MA, Raya M, Kirk N, Erbs K, Spyropoulos P, Nash MS (1994) Energy expenditure of trans-tibial amputees during ambulation at self-selected pace. *Prosthet Orthot Int* 18(2):84–91
53. Mattes SJ, Martin PE, Royer TD (2000) Walking symmetry and energy cost in persons with unilateral transtibial amputations: matching prosthetic and intact limb inertial properties. *Arch Phys Med Rehabil* 81(5):561–568
54. Smith JD, Martin PE (2013) Effects of prosthetic mass distribution on metabolic costs and walking symmetry. *J Appl Biomech* 29(3):317–328